Harmonic Analysis of Pulse Width Modulation-Based Strategies for Modular Multilevel Converter

Imen Ouerdani *‡, Afef Bennani Ben Abdelghani **, Ilhem Slama Belkhodja *

* Université de Tunis El Manar, Ecole Nationale d'Ingénieurs de Tunis LR11ES15 Laboratoire des Systèmes Electriques, 1002, Tunis, Tunisie ;

** Université de Carthage, Institut national des sciences appliquées et de technologie, Tunis 1080, Tunisie

(imen.wardani@gmail.com, afef.bennani@gmail.com, ilhem.slamabelkhodja@gmail.com)

‡ Corresponding Author; Imen Ouerdani, BP 37, Le Belvédère, 1002 Tunis, Tunisia, Tel: +21671874700 Fax: +21671872729. imen.wardani@gmail.com

Received: 03.06.2016 Accepted:05.07.2016

Abstract- MMC converters are an interesting solution for HVDC applications and renewable energy transport. This paper presents a mathematical analysis of the impact of various Phase Disposition PWM strategies on the circulating current which is one of the important MMC converter issues. The considered strategies are: Phase Disposition PWM (PDPWM), Phase Opposition Disposition PWM (PODPWM) and Alternative Phase Opposition Disposition PWM (APODPWM). Depending on the adapted modulation strategy, the proposed analysis proves that the circulating current varies from a DC component to a high current with high frequency components and a dominance of the second order harmonics. It is also demonstrated that PODPWM and APODPWM modulation strategies satisfy the balanced operation condition where only N sub-modules among the 2N available sub-modules are inserted into the phase leg and consequently ensure (N+1) voltage levels in the output voltage. Simulation results of a 2.7 MVA MMC converter are presented to verify the validity of the proposed methodology and analysis.

Keywords Modular Multilevel Converter; circulating current; THD; Pulse Width Modulation.

1. Introduction

With the beginning of a new era of energy production based on distributed energy resources and the need to build a smarter grid [1,2], High Voltage Direct Current (HVDC) is expected to be the method of choice of power transmission [3,4]. HVDC is considered advantageous compared to ac transmission due to its stability when connecting asynchronous ac grids, the great ease of active power control in the DC link and the low power losses even over very long distances [5,6]. These advantages make the HVDC a perfect candidate for grid integration of renewable energy where resources are usually located far from their consumption centres.

Along with the modifications made on conventional centralized electric grids, power conversion attracted major investigations. New topologies were proposed to fit specific applications according to the voltage and power rates [7,8]. The Modular Multilevel Converter (MMC) has emerged as one of the most promising topologies in high voltage high power applications [9,10,11]. The MMC offers various advantages such as low harmonic distortion of the output voltage, low switching frequency, fault tolerant operation, etc. The modularity and scalability of this topology allowed it to reach high voltage ranges with very high number of voltage levels by a simple series connection of conventional sub-modules. Due to this criterion, the MMC has become especially attractive for HVDC transmission and power systems applications [12,13].

Since its introduction by R. Marquardt in 2001[14], extensive researches have been performed to improve the converter's performance regarding its different aspects. In fact, first investigations were dedicated to the topology modelling [15] and dedicated modulation schemes [9],[16]. In [17] and [18], the authors adopted the nearest level control (NLC) also known as the round method. It is especially interesting for MMC with large number of sub-modules [19]. Space Vector PWM (SVPWM) modulation was also applied

for MMC converters [20, 21]. This strategy has the advantage of a higher DC bus utilization ratio and more degrees of freedom; however, its implementation becomes complicated for high number of levels. The modularity and simple implementation of PWM-based modulation strategies make them the most suitable for MMC converters [22]. In [19,21] the high performances of the Carrier Disposition PMW (CDPWM) modulations versus the Phase Shifted Carrier PWM (PSCPWM) methods are detailed.

Nevertheless, the MMC topology requires further control objectives in addition to those of a conventional voltage source converter. Indeed, one of the main issues of the MMC topology is the circulating current. Since upper and lower arms are connected in series, the voltage difference creates a current that flows within the phase units [23] [24]. The so called circulating current flows through the power devices as well as the sub-modules capacitors without having any impact on the ac-side voltages and currents [25]. However, it increases the peak values of upper and lower arm currents and consequently increases the rated current of power devices which further increases the system cost and power losses [26]. Also, the circulating current perturbs the capacitor voltage balancing of the sub-module capacitors and requires, consequently, a more sophisticated balance control algorithm [25].

Circulating current control has been the subject of various researches. In [26],[27],28], various dedicated control algorithms are investigated to suppress the second order harmonic considered as the dominant component of the circulating current spectrum. Although they lead to a sensitive circulating current reduction, the proposed algorithms lead to a non-negligible control complication and limit the extra degrees of freedom of the MMC topology, which may be used to enhance further performances.

The aim of this paper is to analyse the impact of PWM based modulation strategies on the circulating current and evaluate how the PWM technique could enhance the circulating current issue without considering it as an additional constraint. Unlike other multilevel topologies, the MMC converter offer a number of output voltage levels that depend not only on the semi-conductor devices number used to build the converter, but also on the adapted modulation scheme. The proposed analysis is based on the double Fourier integral method to demonstrate which PWM-based modulation strategies are the best adapted to control the MMC converter while eliminating the circulating current.

The paper is organized as follows: in section 2, the model of a three phase MMC converter and the circulating current are introduced. The impact of the Phase Disposition PWM modulation strategies on the converter's performance is analyzed in section 3. Section 4 presents the simulation results and is followed by conclusions in section 5.

2. MMC Converter: Operation Principles and Modelling

A three phase MMC converter topology is depicted in fig.1. Each of its legs is composed by two identical arms. Each arm consists of a series connection of *N* identical sub-modules (*SM*) and an inductor *L*. Different structures can be used to build the sub-modules. In this paper, a sub-module is a Half Bridge converter, as shown in fig.1. The dc side of the converter is modelled by two dc voltage sources $V_{dc}/2$. In the following, such a converter is labelled *N-SM MMC* converter.

Sub-modules are bypassed or inserted in a sinusoidal manner depending on the upper switch control signal *Si*: If *Si=1*, (i.e. the upper switch is ON), the SM is inserted and contributes in the output voltage with its capacitor voltage. The capacitor is charged or discharged according to the arm current sign. If *Si=0*, (i.e. the upper switch is OFF) the SM is bypassed and its output voltage is null. The corresponding capacitor voltage is constant. Bypassing or inserting a given SM depends on two main criteria: realizing the required output voltage while maintaining the capacitors voltages balanced. In this paper, the capacitor value is considered balanced, equal to V_{dc}/N.

Kirchhoff voltage law applied to leg *a* gives:

$$\frac{V_{dc}}{2} - V_{a,u} - L.\frac{di_{a,u}}{dt} - V_a = 0 \quad (1)$$

$$\frac{V_{dc}}{2} - V_{a,l} - V_{L,l} + V_a = 0 \quad (2)$$

where $V_{a,u}$ and $V_{a,l}$ are the upper and the lower arm inductor voltages. They are expressed as:

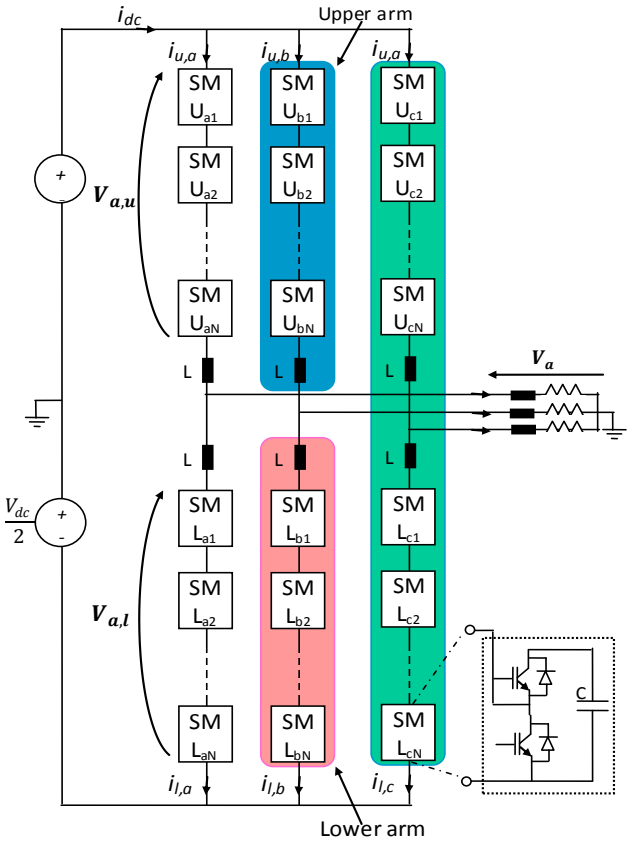

Fig. 1. Topology of an N-SM MMC converter

$$V_{a,u} = \sum_i Si_u V_c = \sum_i Si_u . \frac{V_{dc}}{N} = \frac{n_u}{N} V_{dc} \quad (3)$$

$$V_{a,l} = \sum_i Si_l V_c = \sum_i Si_l . \frac{V_{dc}}{N} = \frac{n_l}{N} V_{dc} \quad (4)$$

where n_u and n_l are the number of inserted sub-modules in the upper and lower arm respectively.

The subtraction of (2) from (1) gives:

$$2V_a + V_{a,u} - V_{a,l} - L.\frac{di_{a,l}}{dt} + L.\frac{di_{a,u}}{dt} = 0 \quad (5)$$

Considering the symmetry of the converter, the leg output current is equally split among the upper and lower arms. Consequently, upper and lower inductor voltages are equal as expressed in (6).

$$L.\frac{di_{a,u}}{dt} = L.\frac{di_{a,l}}{dt} = V_L \quad (6)$$

Inserting (6) in (5) yields to (7).

$$V_a = \frac{V_{a,l} - V_{a,u}}{2} \quad (7)$$

Kirchhoff current law applied to leg *a* gives:

$$i_a = i_{a,u} - i_{a,l} \quad (8)$$

(7) and (8) show that the voltage and current outputs are given by the instantaneous difference between the lower and upper voltages and currents.

Similarly, the sum of (1) and (2) gives:

$$V_L = L.\frac{d(i_{a,u} + i_{a,l})}{2dt} = \frac{V_{dc} - (V_{a,u} + V_{a,l})}{2} \quad (9)$$

According to (7), the inductor compensates the difference between the dc bus and the sum of the upper and lower arms voltages. This instantaneous voltage difference generates the circulating current i_{za}, which flows in the upper arm, lower arm and the dc bus. Current i_{za} has no influence on the output current i_a and is expressed as:

$$i_{za} = \frac{i_{a,u} + i_{a,l}}{2} \quad (10)$$

Inserting (3) and (4) in (9) yields to:

$$V_L = \frac{V_{dc}}{2.N}.(N - (n_u + n_l)) \quad (11)$$

Ideally, the dc bus and the converter's legs are balanced and the inductor voltage is null. Hence, the converter's balance condition is derived from (11) and can be written as:

$$N = n_u + n_l \quad (12)$$

Thus, for a correct *N-SM MMC* converter operation, the modulation strategy has to ensure that *N* SMs among the *2N* available ones are inserted.

Under this condition, (1) an (2) become:

$$V_{a,u} = \frac{V_{dc}}{2} - V_a \quad (13)$$

$$V_{a,l} = \frac{V_{dc}}{2} + V_a \quad (14)$$

As in grid connected generation systems and motor drive field, where the MMC is used in DC/AC operation mode, leg *a* voltage reference is defined as:

$$V_{a,ref} = m.\frac{V_{dc}}{2}\cos(2\pi ft) \quad (15)$$

where *m* is the modulation index.

Consequently, upper and lower arm voltage references are 180° phase shifted.

3. Harmonic Analysis of Level Shifted PWM Strategies and Their Effect on Circulating Current for MMC Converter

The harmonic analysis of voltage and current outputs can be performed using double Fourier integral method [29,30]. In [30], Holmes deeply analyzed PWM based modulation strategies for multilevel converters. The provided quantifications can be simply applied for MMC converters. In fact, the upper and lower arms can be considered as two separated multilevel converters. Each of the considered converters is controlled by an independent PWM block.

3.1. Harmonic Analysis for PDPWM Modulation Strategy

Phase Disposition PWM modulation strategy consists in the comparison of the reference with carriers that are defined with the same magnitude, frequency and phase. They are V_{dc}/N level shifted and form contiguous bands that cover all the linear modulation range. Each carrier is associated to a single sub-module. Upper arm control signals are obtained by comparing the carriers with the upper arm voltage reference. Similarly, lower arm control signals are the comparison result of the carriers with the lower arm voltage reference. On the basis of [30], one arm output voltage $V_{arm}(t,\varphi)$ can be expressed as follows:

$$\begin{aligned} V_{arm}(t,\varphi) &= \frac{V_{dc}}{2} + \frac{V_{dc}}{2}.m.\cos(\omega_0 t + \varphi) + \\ &\frac{2V_{dc}}{N.\pi^2}.\sum_{i=1}^{\infty}\frac{1}{2i}\sum_{j=-\infty}^{\infty} C_e.\cos\left(2i\,\omega_c t + [2j-1][\omega_0 t + \varphi]\right) \\ &+ \frac{4V_{dc}}{N.\pi^2}\sum_{i=1}^{\infty}\frac{1}{2i-1}\sum_{j=-\infty}^{\infty}\sum_{k=1}^{\infty} C_0.\cos\left([2i-1]\omega_c t + 2i\,[\omega_0 t + \varphi]\right) \end{aligned} \quad (16)$$

where:

φ is the initial phase angle of reference waveform, *i* is the carrier index and *j* is the baseband index. w_c and w_0 are the angular frequency of the carrier and the reference respectively.

$$C_0 = J_{2k-1}\left([2i-1]\frac{N}{2}\pi m\right)\cos(k\pi)\times(A+B) \quad (17)$$

$$C_e = \pi J_{2i-1}(iN\pi m).\cos([j-1]\pi) \quad (18)$$

A and *B* are defined in (19) and (20) as in [31].

$$A = \frac{\cos(i-k)\pi - 2.\sum_{h=1}^{N/2-1}\sin\left([2k-2i-1].\cos\left(\frac{2h}{Nm}\right)^{-1}\right).\cos(h\pi)}{2k-2i-1} \quad (19)$$

$$B = \frac{\cos(i+k)\pi - 2\sum_{h=1}^{N/2-1}\sin\left([2k+2i-1].\cos\left(\frac{2h}{Nm}\right)^{-1}\right).\cos(h\pi)}{2k+2i-1} \quad (20)$$

Replacing φ with 0 for the upper arm reference and 180° for the lower arm reference, $V_{a,u}$ and $V_{a,l}$ can be deduced from (16) and are expressed as:

$$\begin{aligned} V_{a,u}(t) &= V_{arm}(t,0) = \frac{V_{dc}}{2} + \frac{V_{dc}}{2}.m.\cos(\omega_0 t) \\ &+ \frac{2V_{dc}}{N\pi^2}.\sum_{i=1}^{\infty}\frac{1}{2i}\sum_{j=-\infty}^{\infty}C_e.\cos\left(2i\,\omega_c t + [2j-1]\omega_0 t\right) \\ &+ \frac{4V_{dc}}{N\pi^2}\sum_{i=1}^{\infty}\frac{1}{2i-1}\sum_{j=-\infty}^{\infty}\sum_{k=1}^{\infty}C_0.\cos\left([2i-1]\omega_c t + 2i\,\omega_0 t\right) \end{aligned} \quad (21)$$

$$\begin{aligned} V_{a,l}(t) &= V_{arm}(t,180) = \frac{V_{dc}}{2} - \frac{V_{dc}}{2}.m.\cos(\omega_0 t) \\ &- \frac{2V_{dc}}{N\pi^2}\sum_{i=1}^{\infty}\frac{1}{2i}\sum_{j=-\infty}^{\infty}C_e.\cos\left(2i\,\omega_c t + [2j-1]\omega_0 t\right) \\ &+ \frac{4V_{dc}}{N\pi^2}\sum_{i=1}^{\infty}\frac{1}{2i-1}\sum_{j=-\infty}^{\infty}\sum_{k=1}^{\infty}C_0.\cos\left([2i-1]\omega_c t + 2i\,\omega_0 t\right) \end{aligned} \quad (22)$$

Inserting (21) and (22) in (9) yields to:

$$V_L = -\frac{4V_{dc}}{N\pi^2}\sum_{i=-\infty}^{\infty}\frac{1}{2i-1}\sum_{\substack{j=-\infty\\ j\neq 0}}^{\infty}\sum_{k=1}^{\infty}C_0.\cos\left([2i-1]\omega_c t + 2j\,\omega_0 t\right) \quad (23)$$

The circulating current expression is deduced from the integration of (23) and expressed as:

$$\begin{aligned} i_z(t) &= \frac{4V_{dc}}{LN\pi^2}\sum_{i=-\infty}^{\infty}\frac{1}{2i-1} \\ &\times\left(\sum_{\substack{j=-\infty\\ j\neq 0}}^{\infty}\sum_{k=1}^{\infty}\frac{C_0}{(2i-1).\omega_c + 2j\,\omega_0}.\cos\left([2i-1]\omega_c t + 2j\,\omega_0 t + \frac{\pi}{2}\right)\right) \end{aligned} \quad (24)$$

Consequently, even carrier harmonics are cancelled from the circulating current harmonic content. The circulating current contains only odd carrier multiples, while sidebands harmonics appear around odd carrier multiples. Also, it is to note that the second order harmonic is the dominant component in the circulating current spectrum.

3.2. Harmonic Analysis for APODPWM Modulation Strategy

Similarly, the analytical solution of one arm output voltage $V_{arm}(t,\varphi)$ is deduced from the multilevel converter leg voltage when modulated with APODPWM [30,31] and is expressed as:

$$\begin{aligned} V_{arm}(t,\varphi) &= \frac{V_{dc}}{2} + \frac{V_{dc}}{2}.m.\cos(\omega_0 t + \varphi) \\ &+ \frac{2V_{dc}}{N\pi}\sum_{i=1}^{\infty}\frac{1}{i}\sum_{\substack{j=-\infty\\ j\neq 0}}^{\infty}J_{2j-1}\left(i\frac{N}{2}\pi m\right)\cos(i\pi)\times\sin\left([Ni+2j-1]\frac{\pi}{2}\right) \\ &\times\cos\left(i\,\omega_c t + [2j-1][\omega_0 t + \varphi]\right) \end{aligned} \quad (25)$$

Thus,

$$\begin{aligned} V_{a,u} &= V_{arm}(t,0) = \frac{V_{dc}}{2} + \frac{V_{dc}}{2}.m.\cos(\omega_0 t) \\ &+ \frac{2V_{dc}}{N\pi}\sum_{i=1}^{\infty}\frac{1}{i}\sum_{\substack{j=-\infty\\ j\neq 0}}^{\infty}J_{2j-1}\left(i\frac{N}{2}\pi m\right)\times\cos(i\pi)\times\sin\left([Ni+2j-1]\frac{\pi}{2}\right) \\ &\times\cos\left(i\,\omega_c t + [2j-1]\omega_0 t\right) \end{aligned} \quad (26)$$

And

$$\begin{aligned} V_{a,l} &= V_{arm}(t,180) = \frac{V_{dc}}{2} - \frac{V_{dc}}{2}.m.\cos(\omega_0 t) \\ &- \frac{2V_{dc}}{N\pi}\sum_{i=1}^{\infty}\frac{1}{i}\sum_{\substack{j=-\infty\\ j\neq 0}}^{\infty}J_{2j-1}\left(i\frac{N}{2}\pi m\right)\times\cos(i\pi)\times\sin\left([Ni+2j-1]\frac{\pi}{2}\right) \\ &\times\cos\left(i\,\omega_c t + [2j-1]\omega_0 t\right) \end{aligned} \quad (27)$$

Inserting (26) and (27) into (9) gives an inductor voltage that is equal to zero. This means that APODPWM ensures a correct converter operation where circulating current is constant and the inserted sub-modules number is equal to *N*. Consequently, the converter's output voltage step is equal to V_{dc}/N and *(N+1)* voltage levels can be generated.

3.3. Harmonic Analysis for PODPWM Modulation Strategy

PODPWM leads to the arm output voltage that is expressed as:

$$\begin{aligned} V_{arm}(t,\varphi) &= \frac{V_{dc}}{2} + \frac{V_{dc}}{2}.m.\cos(\omega_0 t + \varphi) \\ &+ \frac{2V_{dc}}{N\pi}\sum_{i=1}^{\infty}\frac{1}{2i}\sum_{j=-\infty}^{\infty}J_{2j-1}(iN\pi m)\times\cos(i\pi) \\ &\times\cos\left(2m\,\omega_c t + [2j-1](\omega_0 t + \varphi)\right) \\ &+ \frac{2V_{dc}}{N\pi^2}\sum_{i=1}^{\infty}\frac{1}{2i-1}\sum_{j=-\infty}^{\infty}(C+D) \\ &\times\cos\left((2i-1)\omega_c t + [2j-1][\omega_0 t + \varphi]\right) \end{aligned} \quad (28)$$

C and *D* are defined as:

$$C = J_{2j-1}(i\pi Nm)\frac{2\pi m}{N}\times\cos(j\pi)\times\frac{\pi}{2}-2\theta-\frac{\sin(2(2j-1)\theta)}{(2j-1)}$$
$$+\frac{2V_{dc}}{N\pi}\sum_{i=1}^{\infty}\frac{1}{i}\sum_{\substack{j=-\infty\\ j\neq 0}}^{\infty}J_{2j-1}\left(i\frac{N}{2}\pi m\right)\times\cos(i\pi)\times\sin\left(\left[Ni+2j-1\right]\frac{\pi}{2}\right) \quad (29)$$
$$\times\cos\left(i\omega_c t+\left[2j-1\right]\omega_0 t\right)$$

And

$$D=\sum_{\substack{k=1\\ k\neq j\\ k\neq j+1}}^{\infty}\begin{matrix}J_{2k-1}\times\left((2j-1).2\pi.\frac{m}{N}\right)\times\cos(k\pi)\\ \times 2\left(\frac{\sin(2k-2j).\theta}{2k-2j}+\frac{\sin(2k-2j-2).\theta}{2k-2j-2}\right)\end{matrix} \quad (30)$$

where $\theta=\cos\left(\frac{1}{2m}\right)^{-1}$

Upper and lower arm voltage expressions are respectively given by (31) and (32):

$$V_{a,u}(t)=V_{arm}(t,0)=\frac{V_{dc}}{2}+\frac{V_{dc}}{2}.m.\cos(\omega_0 t)$$
$$+\frac{2V_{dc}}{N\pi}\sum_{i=1}^{\infty}\frac{1}{2i}\sum_{j=-\infty}^{\infty}J_{2j-1}.(iN\pi m)\times\cos(i\pi)$$
$$\times\cos\left(2m\omega_c t+\left[2j-1\right](\omega_0 t)\right) \quad (31)$$
$$+\frac{2V_{dc}}{N\pi^2}\sum_{i=1}^{\infty}\frac{1}{2i-1}\sum_{j=-\infty}^{\infty}(A+B)\times\cos\left(\begin{matrix}(2i-1)\omega_c t\\ +\left[2j-1\right].\left[\omega_0 t\right]\end{matrix}\right)$$

$$V_{a,l}(t)=V_{arm}(t,180)=\frac{V_{dc}}{2}-\frac{V_{dc}}{2}.m.\cos(\omega_0 t)$$
$$-\frac{2V_{dc}}{N\pi}\sum_{i=1}^{\infty}\frac{1}{2i}\sum_{j=-\infty}^{\infty}J_{2j-1}.(iN\pi m)\times\cos(i\pi)$$
$$\times\cos\left(2m\omega_c t+\left[2j-1\right](\omega_0 t)\right) \quad (32)$$
$$-\frac{2V_{dc}}{N\pi^2}\sum_{i=1}^{\infty}\frac{1}{2i-1}\sum_{j=-\infty}^{\infty}(A+B)\times\cos\left(\begin{matrix}(2i-1)\omega_c t\\ +\left[2j-1\right].\left[\omega_0 t\right]\end{matrix}\right)$$

Summing $V_{a,u}(t)$ and $V_{a,l}(t)$ and subtracting the result from the dc bus gives a null inductor voltage. Hence, the circulating current is constant. PODPWM also generates ($N+1$) voltage level in the converter's output voltage.

4. Simulation Results of a 4-SM MMC Converter

To verify the above analysis, computer simulations of a 4-SM MMC 2.7 MVA converter were performed using PSIM software. The circuit parameters are summarized in Table I.

Table 1. Simulated circuit parameters

Parameter	Value
DC bus	8000V
Arm inductance	100µH
Carrier frequency	10 kHz
Carrier peak to peak	2000V
Load resistance	11Ω
Load inductance	10mH
Modulation ratio	0.9

Firstly, the converter is controlled by PDPWM. All carriers have the same initial phase angle, equal to zero as shown in fig. 2.

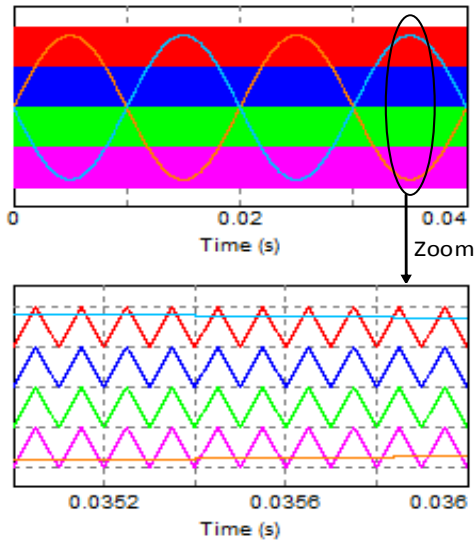

Fig. 2. PDPWM for a 4-SM MMC converter

The three line output currents are depicted in fig. 3. They form a balanced three phase system with 338 A as maximum value and a THD equal to 0.07%.

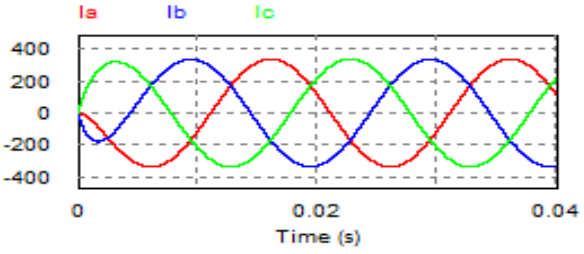

Fig. 3. Phase *a*, *b* and *c* currents of a PDPWM modulated 4 SM-MMC converter

The line to neutral output voltages V_{ao}, V_{bo} and V_{co} are presented in fig. 4. Each phase presents 9 voltage levels with a THD equal to 16.7%.

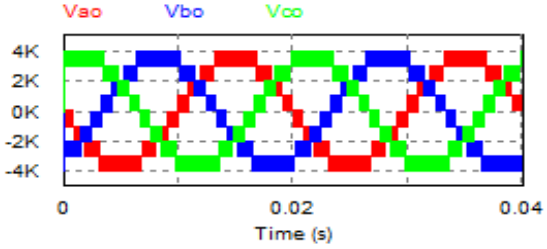

Fig. 4. Line to neutral output voltages of a PDPWM modulated 4-SM MMC converter

Leg *a* output circulating current i_{za} and upper arm inductor voltage are depicted in fig. 5. Inductor voltage oscillates between -1kV and +1kV at the switching frequency. Consequently, the circulating current amplitude reaches high values (over 250A) as shown in fig.5-b.

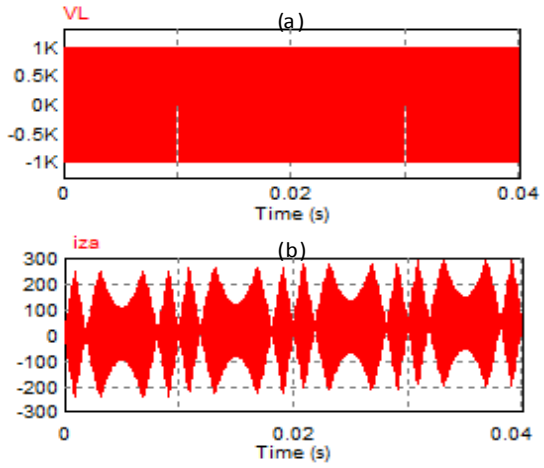

Fig. 5. Leg *a* outputs a) upper arm inductor voltage b) circulating current i_{za} temporal analysis

As demonstrated in (24), circulating current spectral analysis shows high frequency components, odd multiple of the switching frequency and sidebands that are odd multiple of the modulation frequency. Accordingly, fig. 6 shows that first carrier harmonics appear at the switching frequency, 10 kHz, with fundamental even multiple sidebands harmonics at 9900Hz and 10100. The next harmonics appear at 30 kHz, with sidebands harmonics at 29800 Hz, 29900 Hz, 30100Hz and 30200 Hz (fig. 6).

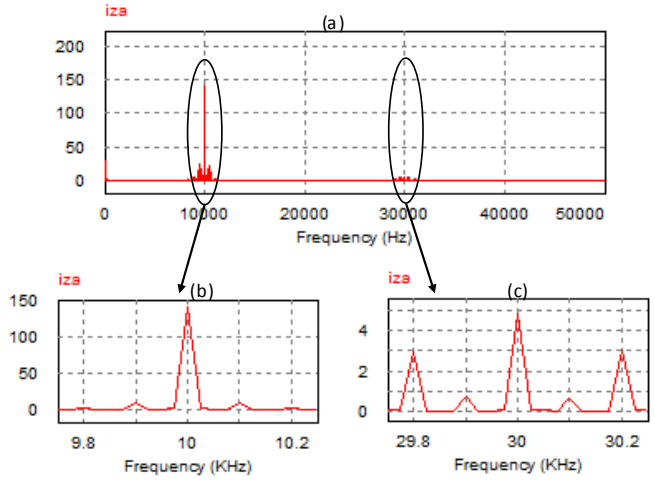

Fig. 6. Spectral analysis for leg *a* circulating currents a) simulation result over 50 kHz b) zoom around 10 kHz c) zoom around 20 kHz

Second modulation strategy used for the converter's control is the APODPWM. Neighbouring carriers are 180° phase shifted. Hence, they are symmetric to the voltage reference average value as shown in fig. 7.

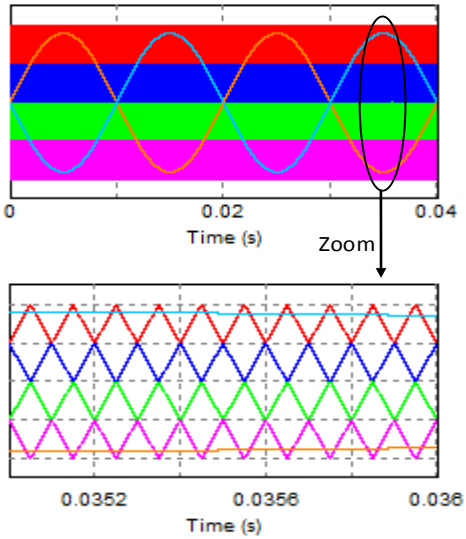

Fig. 7. APODPWM for a 4-SM MMC converter

Fig.8 shows phase *a* output current where the THD is equal to 0.36%.

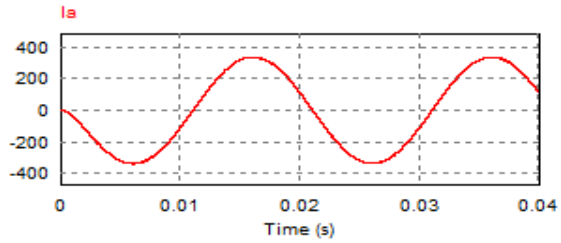

Fig. 8. Phase *a* current of APODPWM modulated 4 SM-MMC converter

Leg *a* output voltage depicted in fig. 9 shows 5 levels: -4 kV, -2 kV, 0 V, 2 kV and 4 kV. Calculated THD voltage is equal to 33.3%.

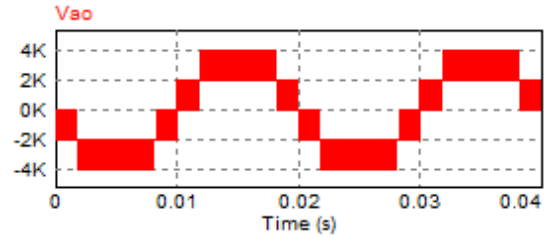

Fig. 9. Leg *a* output voltage obtained with APODPWM: 5 levels

APODPWM ensures the insertion of exactly *N* sub-modules among the *2N* available ones. For the considered 4-SM MMC converter, 4 sub-modules are inserted while the 4 remaining ones are disconnected. The DC bus is then equally divided into the 4 inserted sub-modules, resulting in 5 output voltage levels.

Hence, the inductor voltage is low, with a maximum value equal to 10V for a 0.5% rate compared to one voltage step. The circulating current is a dc component, with an average value equal to 22mA as shown in fig. 10.

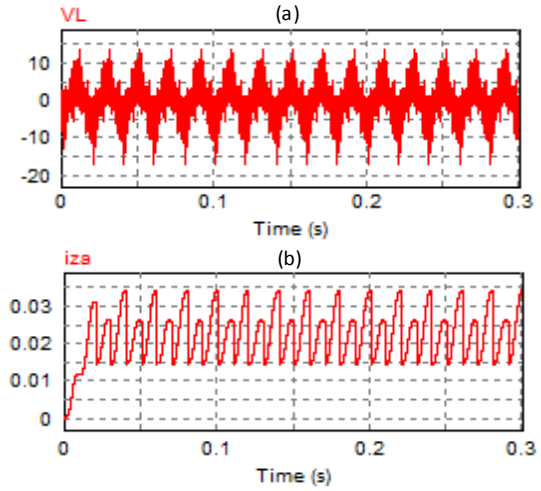

Fig. 10. Leg *a* outputs a) upper arm inductor voltage b) circulating current

Finally, the 4-SM MMC converter is controlled with PODPWM modulation strategy. Carriers are symmetric according to the reference average value. The two upper carriers have a null initial phase angle, whereas the two lower carriers are 180° phase shifted as shown in fig. 11.

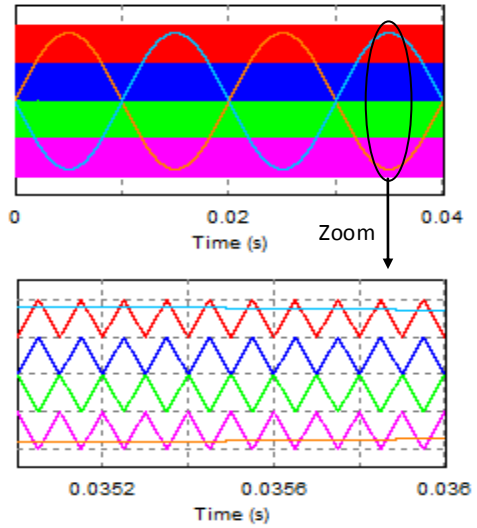

Fig. 11. PODPWM for a 4-SM MMC converter

Leg *a* current and voltage outputs are shown on fig. 12 and fig. 13 respectively. Current THD is equal to 0.37% and voltage THD is equal to 33.3%.

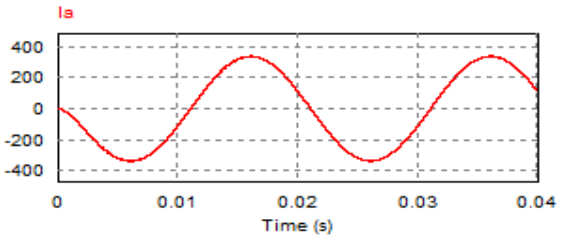

Fig. 12. Line a current of PODPWM modulated 4 SM-MMC converter

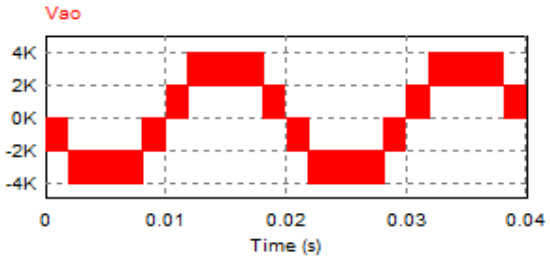

Fig. 13. Leg a output voltage obtained with PODPWM: 5 levels

Similarly to the APODPWM, inductor voltage is negligible, circulating current is low and the number of the inserted SM is equal to 4, as shown in fig. 14, fig.15 and fig.16 respectively.

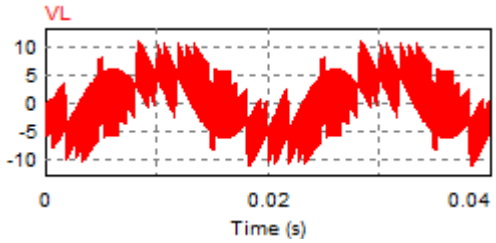

Fig. 14. Leg *a* upper arm inductor voltage

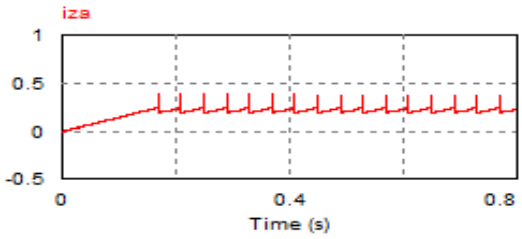

Fig. 15. Phase *a* circulating current

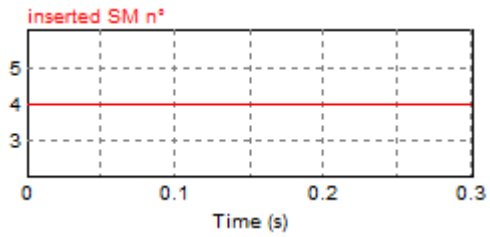

Fig. 16. Number of inserted SM with PODPWM

In order to evaluate the considered modulation strategies performances, the converter's current and voltage outputs are analysed and compared to the current and voltage harmonics standards established according to IEC TR 61000-3-6: 2008 [32]. In fact, the MMC converter is mainly used in HVDC transmission systems [33]. Furthermore, considering its inherent advantages, the MMC topology would be extended for energy distribution application [34]. In both cases, considering the pulse-width-modulated output voltages, a filter is required to connect the converter to the grid. Therefore, the key challenge is to reduce the filter's size, cost and resulting power losses.

According to IEC TR 61000-3-6: 2008, the current harmonics standards are equal to 1.2% for distribution lines and 0.4% for transmission ones. Voltage harmonics standards are equal to 1.5% for bus voltage at PCC greater than 161 kV. The voltage THD for high voltage systems like in HVDC applications is limited to 2%.

For the three proposed modulation strategies of MMC converters, current THD does not exceed 0.33%. Consequently, the line currents verify the current harmonics standards. Due to the greater number of the output voltage levels obtained with PDPWM compared to PODPWM and APODPWM, the obtained voltage THD, equal to 16.7%, is lower than the one obtained with PODPWM and APODPWM strategies, equal to 33.3%. As expected, the three proposed modulation strategies achieve a low THD in the converter's output voltage. The lower the THD is, the more optimised the filter is. Even though the voltage THD seems to exceed the aforementioned standards, it is to note that it will be sensitively reduced if a filter is added into the system.

5. Conclusion

This paper investigated the circulating current harmonics for an N-SM MMC converter. A double Fourier integral based methodology was proposed to point out the effect of the converter modulation technique on the circulating current harmonics. . It has been showed that the circulating current harmonic is a DC component when the converter is controlled with PODPWM and APODPWM strategies. Under these conditions, the converter operates in balanced conditions between the phase legs and the DC bus. This balance ensures that exactly N sub-modules are inserted into the leg and consequently (N+1) voltage levels exist in the output voltage of the corresponding leg. Whereas, when the converter is controlled with PDPWM, the circulating current reaches high values with high frequency harmonics that are odd multiple of the switching frequency. Hence, the circulating current harmonics can be fully eliminated and its magnitude can be tremendously reduced when using the appropriate modulation strategy. Extra degrees of freedom can then be exploited to solve other issues of the MMC converter, namely the sub-modules capacitors voltage balance.

References

[1] V. Ramesh and S. Mandava, "Microgrid Design and Control Using a Discrete Proportional Resonant Controller," *Int. J. Renew. Energy Res. IJRER*, vol. 5, no. 4, pp. 1041–1048, December 2015.

[2] G. N. Prodromidis, L. Kikareas, P. Stamatopoulou, G. Tsoumanis, and F. A. Coutelieris, "Modelling and Experimental Study on Renewable Energy Based Hybrid Systems," *Int. J. Renew. Energy Res. IJRER*, vol. 5, no. 4, pp. 1186–1195, December. 2015.

[3] J. Vobecky, V. Botan, K. Stiegler, M. Bellini, and U. Meier, "New Low Loss Thyristor for HVDC Transmission," in *Renewable Energy and Energy Management; Proceedings of PCIM Europe 2015; International Exhibition and Conference for Power Electronics, Intelligent Motion*, Nuremberg, pp. 1–6, 19-21 May 2015.

[4] O. Alizadeh-Mousavi, C. Y. Evrenosoglu, and M. Zima-Bockarjova, "Optimal location and sizing of HVDC converters for same-tower AC-DC overhead lines," in *PowerTech, 2015 IEEE Eindhoven*, 29 June-2 July 2015, pp. 1–6.

[5] S. Acharya, S. Bhattacharya, and N. Yousefpoor, "Dynamic performance evaluation of hybrid multi-terminal HVAC/HVDC grid," in *2015 IEEE Energy Conversion Congress and Exposition (ECCE)*, 20-24 September 2015, pp. 2287–2293.

[6] J.S. Contreras, and F. Rivas Davalos, "Reliability and availability of VSC-HVDC links: A state of the art.", 2015 IEEE International Autumn Meeting on Power, Electronics and Computing (ROPEC), 4-6 November 2015, pp. 1-8

[7] E. Behrouzian, M. Bongiorno, and H. Z. D. L. Parra, "An overview of multilevel converter topologies for grid connected applications," in *2013 15th European Conference on Power Electronics and Applications (EPE)*, Lille, 2-6 September 2013, pp. 1–10.

[8] P. Qashqai, A. Sheikholeslami, H. Vahedi, and K. Al-Haddad, "A Review on Multilevel Converter Topologies for Electric Transportation Applications," in *2015 IEEE Vehicle Power and Propulsion Conference (VPPC)*, Montreal, 19-22 October 2015, pp. 1–6.

[9] B. Li, R. Yang, D. Xu, G. Wang, W. Wang, and D. Xu, "Analysis of the Phase-Shifted Carrier Modulation for Modular Multilevel Converters," *IEEE Trans. Power Electron.*, vol. 30, no. 1, pp. 297–310, January 2015.

[10] S. Fan, K. Zhang, J. Xiong, and Y. Xue, "An Improved Control System for Modular Multilevel Converters with New Modulation Strategy and Voltage Balancing Control," *IEEE Trans. Power Electron.*, vol. 30, no. 1, pp. 358–371, January 2015.

[11] U. Karaagac, J. Mahseredjian, L. Cai, and H. Saad, "Offshore Wind Farm Modeling Accuracy and Efficiency in MMC-Based Multi-Terminal HVDC Connection," *IEEE Trans. Power Deliv.*, vol. PP, no. 99, pp. 1–1, 2016.

[12] J. Qin and M. Saeedifard, "A Zero-Sequence Voltage Injection-Based Control Strategy for a Parallel Hybrid Modular Multilevel HVDC Converter System," *IEEE Trans. Power Deliv.*, vol. 30, no. 2, pp. 728–736, April 2015.

[13] A. Alexander and M. Thathan, "Modelling and analysis of modular multilevel converter for solar photovoltaic applications to improve power quality," *IET Renew. Power Gener.*, vol. 9, no. 1, pp. 78–88, 2015.

[14] R. Marquardt, "Current rectification circuit for voltage source inverters with separate energy stores replaces

phase blocks with energy storing capacitors," DE10103031A1.

[15] J.-W. Moon, J.-W. Park, D.-W. Kang, and J.-M. Kim, "A Control Method of HVDC-Modular Multilevel Converter Based on Arm Current Under the Unbalanced Voltage Condition," *IEEE Trans. Power Deliv.*, vol. 30, no. 2, pp. 529–536, April 2015.

[16] Z. Zheng and C. Can, "The research of control algorithm and topology for high voltage frequency converter based on modular multilevel converter," in *Control and Decision Conference (2014 CCDC), The 26th Chinese*, Changsha, 31 May - 2 June 2014, pp. 4425–4430.

[17] J. Rodriguez, S. Bernet, B. Wu, J. O. Pontt, and S. Kouro, "Multilevel Voltage-Source-Converter Topologies for Industrial Medium-Voltage Drives," *IEEE Trans. Ind. Electron.*, vol. 54, no. 6, pp. 2930–2945, December 2007.

[18] F. Deng and Z. Chen, "A Control Method for Voltage Balancing in Modular Multilevel Converters," *IEEE Trans. Power Electron.*, vol. 29, no. 1, pp. 66–76, January 2014.

[19] P. M. Meshram and V. B. Borghate, "A Simplified Nearest Level Control (NLC) Voltage Balancing Method for Modular Multilevel Converter (MMC)," *IEEE Trans. Power Electron.*, vol. 30, no. 1, pp. 450–462, January 2015.

[20] Y. Deng, M. Saeedifard, and R. G. Harley, "An optimized control strategy for the modular multilevel converter based on space vector modulation," in *2015 IEEE Applied Power Electronics Conference and Exposition (APEC)*, Charlotte NC, 15-19 March 2015, pp. 1564–1569.

[21] A. Lesnicar and R. Marquardt, "An innovative modular multilevel converter topology suitable for a wide power range," in *Power Tech Conference Proceedings, 2003 IEEE Bologna*, 23-26 June 2003, vol. 3, p. 6 pp. Vol.3–.

[22] B. Li, R. Yang, D. Xu, G. Wang, W. Wang, and D. Xu, "Analysis of the Phase-Shifted Carrier Modulation for Modular Multilevel Converters," *IEEE Trans. Power Electron.*, vol. 30, no. 1, pp. 297–310, January 2015.

[23] X. Yang, J. Li, X. Wang, W. Fan, and T. Q. Zheng, "Circulating Current Model of Modular Multilevel Converter," in *Power and Energy Engineering Conference (APPEEC), Asia-Pacific-Wuhan*, 25-28 March *2011*, pp. 1–6.

[24] Y. Ma, and L. Fan, "Circulating current and DC current ripple control in MMC under unbalanced grid voltage.", North American Power Symposium (NAPS), Charlotte NC, 4-6October 2015, pp.1-6.

[25] S. Debnath, J. Qin, B. Bahrani, M. Saeedifard, and P. Barbosa, "Operation, Control, and Applications of the Modular Multilevel Converter: A Review," *IEEE Trans. Power Electron.*, vol. 30, no. 1, pp. 37–53, January 2015.

[26] X. Li, Q. Song, W. Liu, S. Xu, Z. Zhu, and X. Li, "Performance Analysis and Optimization of Circulating Current Control for Modular Multilevel Converter," *IEEE Trans. Ind. Electron.*, vol. 63, no. 2, pp. 716–727, February 2016.

[27] X. Zhang and P. Wang, "Circulating current analysis and suppression of modular multilevel converters," in *2014 17th International Conference on Electrical Machines and Systems (ICEMS)*, Hangzhou, 22-25 October 2014, pp. 2478–2482.

[28] Z. Chu, Y. Li, P. Wang, Z. Li, F. Gao, and H. Zhu, "A novel circulating current suppressing method of modular multilevel converter," in *Transportation Electrification Asia-Pacific (ITEC Asia-Pacific), 2014 IEEE Conference and Expo*, Beijing, 31 August- 3 September 2014, pp. 1–5.

[29] B. P. McGrath and D. G. Holmes, "An analytical technique for the determination of spectral components of multilevel carrier-based PWM methods," *IEEE Trans. Ind. Electron.*, vol. 49, no. 4, pp. 847–857, August 2002.

[30] D. G. Holmes and T. A. Lipo, *Pulse Width Modulation for Power Converters: Principles and Practice*. John Wiley & Sons, 2003, ch. 11.

[31] X. Liu, A. Lindemann, and H. Amiri, "Theoretical and experimental comparison of different control strategies for modular multilevel converters," in *2014 IEEE 15th Workshop on Control and Modeling for Power Electronics (COMPEL)*, Santander, 22-25 June 2014, pp. 1–9.

[32] International Electrotechnical Commission, "IEC/TR 61000-3-6," Technical Report Edition 2.0 2008-02, Feb. 2008.

[33] S. Cui, J.-J. Jung, Y. Lee, and S.-K. Sul, "A novel control strategy of a modular multilevel converter (MMC) based VSC-HVDC transmission system," in *2015 IEEE Applied Power Electronics Conference and Exposition (APEC)*, 15-19 March 2015, pp. 972–979.

[34] B. Fan, Y. Li, K. Wang, Z. Zheng, and L. Xu, "Hierarchical System Design and Control of a MMC-based Power Electronic Transformer," *IEEE Trans. Ind. Inform.*, vol. PP, no. 99, pp. 1–1, January 2016.